Surface kinetics and plasma equipment model for Si etching by fluorocarbon plasmas

Da Zhang[a] and Mark J. Kushner[b]
University of Illinois, 1406 W. Green Street, Urbana, Illinois 61801

(Received 19 August 1999; accepted for publication 18 October 1999)

Plasma-surface interactions during plasma etching are important in that, in addition to determining the rate and quality of the etch, they can also influence the properties of the bulk plasma. To address this coupling of bulk and surface processes the surface kinetics model (SKM) was developed as a module in the two-dimensional hybrid plasma equipment model (HPEM) with the goal of combining plasma chemistry and surface chemistry in a self-consistent fashion. The SKM obtains reactive fluxes to the surface from the HPEM, and generates the surface species coverages and the returning fluxes to the plasma by implementing a user defined surface reaction mechanism. Although the SKM is basically a surface-site-balance model, extensions to those algorithms have been made to include an overlying passivation layer through which reactants and products diffuse. Etching of Si in an inductively coupled plasma sustained in Ar/C_2F_6 was investigated using the SKM. Results from parametric studies are used to demonstrate the sensitivity of etching rates and polymer thickness to the sticking coefficient of fluorocarbon radicals on the reactor walls, polymer erosion rates and F atom diffusion through the polymer layer. © *2000 American Institute of Physics.* [S0021-8979(00)01903-4]

I. INTRODUCTION

The trend in plasma processing is towards the use of low pressure, high plasma density etching reactors in which reactive species more frequently interact with the chamber walls and the wafer surface compared to their high pressure counterparts.[1] These trends have renewed concern about the consequences of plasma surface interactions on both the behavior of the bulk plasma and on the quality of the etch.[2–6] For example, recent studies were performed by Schaepkens *et al.* in which the wall temperature of the chamber was varied during Si etching using fluorocarbon gases in an inductively coupled plasma (ICP) reactor.[4] They observed that the density of radicals in the gas phase, the thickness of the polymer layer on the wafer, and the etch rate were all functions of the wall temperature. These effects were attributed to the temperature dependence of the sticking coefficient[5] of fluorocarbon radicals on the walls of the chamber. Plasma equipment, surface chemistry, and molecular dynamics models have been successful in separately addressing bulk plasma and surface processes.[7–11] There have, however, been few efforts to date which have self-consistently combined plasma and surface processes to simulate low pressure systems where wall processes may dominate.

In this article, an integrated surface kinetics model and plasma equipment model are described and applied to the investigation of wall reactions on Si etching using C_2F_6 in an ICP reactor. The sensitivity of the model to kinetic parameters is also discussed. The integrated model combines the previously described hybrid plasma equipment model (HPEM)[12,13] with a newly developed surface kinetics module (SKM) in which a modified surface site balance algorithm is employed at all points along the plasma-surface boundary. The SKM accepts fluxes of reactants from the bulk plasma model and produces surface coverages, effective reactive sticking coefficients, and the identities of species returning to the plasma. In doing so, different surface reaction mechanisms can be investigated for different types of materials (or locations) in the reactor. One feature of the fluorocarbon etching of Si is that a polymer passivation layer is formed on the wafer by CF_x radicals.[2,4–6,14,15] The Si etching precursor, F atoms, must diffuse through the layer to reach the Si surface, and etch products must diffuse back through the layer.[5] The modified surface-site-balance model allows for deposition of passivation layers, passivation thickness dependent rates, and transport of reactants through the layer to address these conditions. The integrated model is described in Sec. II followed by a discussion of our results for Ar/C_2F_6 etching of Si in an ICP reactor in Sec. III. Our concluding remarks are in Sec. IV.

II. DESCRIPTION OF THE INTEGRATED MODEL AND REACTION MECHANISMS

The hybrid plasma equipment model (HPEM) is a modeling hierarchy which has been developed to address low temperature, low pressure plasma processing. A detailed discussion of the HPEM can be found elsewhere.[12,13] Briefly, the HPEM is a two- or three-dimensional simulation consisting of three main modules. The electromagnetic module (EMM) calculates electromagnetic fields and magnetostatic fields. These fields are used in the electron energy transport module (EETM) where electron impact source functions and

[a]Department of Materials Science and Engineering; electronic mail: dazhang@uiuc.edu
[b]Department of Electrical and Computer Engineering; electronic mail: mjk@uiuc.edu

transport coefficients are derived. Results from the EETM are transferred to the fluid-chemical kinetics module (FKM) which computes the densities, momentum, and temperatures of plasma species, and solves Poisson's equation for the electrostatic potential. These results are transferred back to the EMM and EETM for another iteration, and the process is repeated until a converged solution is obtained. In this work, continuity, momentum, and energy equations are solved for all neutrals and ions included in the model. Continuity and energy equations are solved for electrons using a drift-diffusion approximation for momentum.

Before the development of the SKM, the HPEM used a fixed boundary condition at the plasma-solid interface. For each plasma species hitting a surface (e.g., wafer, reactor wall or quartz window), a reaction probability S_{im} for the ith plasma species, mth surface material was defined. Computationally, all species are ''consumed'' on all boundaries. Depending on the surface reaction mechanism, species are ''reflected'' back into the plasma. The reflecting flux of the same species back to the bulk plasma from the mth material is

$$\Phi_{\mathrm{im}}^{R}=(1-S_{\mathrm{im}})\Phi_{\mathrm{im}}^{I}, \tag{1}$$

where Φ_{im}^{I} is the flux of species i to the surface m. We also specified that each incident species may produce other species on the surface. So for a species i incident onto surface m, the flux of the jth generated species returning to the plasma is

$$\Phi_{ijm}^{R}=\Phi_{\mathrm{im}}^{I}f_{ijm}, \tag{2}$$

where f_{ijm} is the fractional generation rate. For example, consider an argon ion (species 1) striking a wall passivated by a CF_x polymer (material 4), neutralizing to form ground state Ar (species 2) with unity probability and sputtering CF_2 (species 3) with probability of 0.2 $Ar^+ \xrightarrow{\text{wall}} Ar+CF_2$. The coefficients are $S_{14}=1$, $f_{124}=1$, $f_{134}=0.2$. This method is, in principle, exact provided that all of the S_{im} and f_{ijm} coefficients are specified properly. Since the values of S_{im} and f_{ijm} ultimately depend on surface coverages, and the fluxes and energies of reactants, a surface reaction mechanism is required to specify them, and that is the purpose of the SKM.

The SKM was designed to be a self-consistent module functioning within the HPEM framework. The SKM first identifies specified surface locations on chosen materials, sets the initial surface species coverages, and extracts reactive fluxes to the surface from the HPEM. Based on a specified surface reaction mechanism, differential equations for fractional occupancy of surface sites and thickness of overlaying polymer layers are integrated in time. After reaching the steady state or a specified end time, the resulting coefficients S_{ik} and f_{ijk} are fed back to the HPEM for use as boundary conditions in the manner previously described. These coefficients are held fixed until the next call to the SKM. Etching or deposition rates are obtained based on the surface coverages and reactive fluxes at the end of the call to the SKM.

The surface reaction mechanism for fluorocarbon plasma etching of silicon used here is based on the work of Standaert *et al.*,[5] and is shown schematically in Fig. 1. Briefly, etching of bare silicon results from the adsorption of fluorine atoms

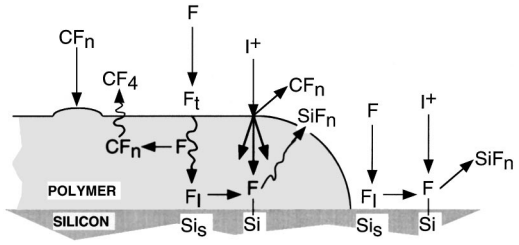

FIG. 1. Schematic of the reaction mechanism for F etching of Si through a polymer layer.

(F) from the plasma onto bare silicon sites (Si_s). The adsorbed fluorine (F_I) then passivates the underlying silicon by chemisorption (=Si–F). Ion bombardment (I^+) provides the activation energy to desorb the etch product (SiF_n). In the presence of a fluorocarbon radical flux (CF_n), a polymer layer is deposited on the silicon. Fluorine atoms adsorb on the top of the polymer (F_T) and diffuse through the polymer where they adsorb on the bare Si sites at the interface (F_I). The adsorbed fluorine passivates the silicon as in the bare case. Ions incident on the polymer disperse energy through the layer to desorb etch products which diffuse back out the layer. The ions also sputter the polymer layer. Fluorine atoms diffusing through the polymer etch the polymer, forming a volatile product (CF_4) which diffuses out the layer.

There are three classes of processes in the surface reaction mechanism. The first class involves reactions of plasma species with surface species or sites. The generic form of these reactions is

$$A_g+B_s\rightarrow C_s+D_g+E_g, \tag{3}$$

where the subscript g denotes a gas phase species and the subscript s denotes a surface resident species or a surface site. The rate of reaction of the ith process of gas species A with surface species B on material m is

$$R_{iABm}=k_{iABm}\Phi_{Am}^{I}\theta_{Bm}, \tag{4}$$

where Φ_{Am}^{I} is the incident plasma flux of species A on M, θ_{Bm} is the fractional surface coverage of surface species or site B on m, and k_{iABm} is the probability of reaction i for incident species A with site or species B on material m. The surface reaction coefficient S_{Am} for incident plasma species A on material m which is used in the bulk plasma model is then the sum of the reaction rates of all processes including A as a reactant,

$$S_{Am}=\sum_{j=1}^{s}\sum_{i=1}^{n}\frac{R_{iAjm}}{\Phi_{Am}^{I}}=\sum_{j=1}^{s}\sum_{i=1}^{n}k_{iAjm}\theta_{jm}, \tag{5}$$

where s is the total number of surface species and n is the number of reactions of A with surface species j. The generation rate for the returning flux of a gaseous reaction product D [Eq. (3)] from material m is then the sum of the rates of all reactions generating D,

$$\Phi_{Dm}^{R}=\sum_{l=1}^{t}\Phi_{lDm}^{R}=\sum_{l=1}^{t}\sum_{j=1}^{s}\sum_{i=1}^{n}\sum_{p=1}^{q}k_{iljm}\Phi_{lm}^{I}\theta_{mj}\delta(p-D), \tag{6}$$

where t is the total number of gas phase species and q is the number of products of that reaction. The returning flux coefficient from material m is then

$$f_{ADm}=\sum_{j=1}^{s}\sum_{i=1}^{n}\sum_{p=1}^{q} k_{iAjm}\theta_{jm}\delta(p-D). \tag{7}$$

The rate coefficients for surface reactions with ions may be functions of ion energy. The rate of reaction is typically characterized by a threshold energy and an exponential[16]

$$p(E)=p_0\frac{E^m-E_{\text{th}}^m}{E_{\text{ref}}^m-E_{\text{th}}^m}, \tag{8}$$

where $p(E)$ is the reaction probability for an ion with energy E, E_{th} is the threshold energy of the process, E_{ref} is a reference energy, and p_0 is the reaction probability at the reference energy. Typically, $m=1/2$ for sputtering or ion activated etching, and that value was used in this work. In this version of the HPEM, we are not explicitly computing the kinetic energy of individual ions. The ion energy used in $p(E)$ is an average value obtained in the following manner. The sheath voltage drop (V_s) at each surface location is estimated by taking the difference between the local plasma and surface potential. The sheath thickness (t_s) at a given surface location is determined by searching for the nearest location to the surface where quasi-neutrality is achieved. We approximate the quasi-neutral condition as

$$\frac{|\Sigma_i(q_i n_i)-n_e|}{n_e}\leqslant 5\%, \tag{9}$$

where n_i is the ion density, q_i is the charge of the ion, n_e is the electron density. Assuming collisions are totaling energy dissipating, the energy (E_i) of the incident species i is estimated by

$$E_i=\text{Min}\left(1,\frac{\lambda_i}{t_s}\right)V_s, \tag{10}$$

where λ_i is the mean free path of the species.

The second class of reactions in the mechanism is between surface species or surface sites. For example,

$$=\text{Si}-\text{F}_s+=\text{Si}-\text{F}_s\rightarrow \text{F}_{2(g)}+=\text{Si}-+=\text{Si}- \tag{11}$$

denotes the interconnection of two fluorine passivated silicon surface sites, evolving molecular fluorine, and producing two bare Si sites. The rates of reaction for these processes are $k\,\theta_{\text{F}}\,\theta_{\text{F}}$, where k is the rate coefficient.

The third class of reactions is deposition of multiple layers of passivation and transport of species through those layers. For example, during fluorocarbon etching of Si, CF_x radicals deposit on the wafer surface to form a polymer layer. The thickness of this layer regulates the etch rate.[5] F atoms, the precursor for Si etching, must diffuse through the CF_x passivation layer, and so thicker layers imply lower diffusion rates and lower Si etching rates. Similarly, thicker passivation layers disperse incident ion energy before its delivery to the surface to activate desorption processes.

The SKM represents the deposition of passivation layers and the etching of underlying Si in the following manner. CF_x radicals from the plasma are the source material for growth of the passivation layer. The bombardment by energetic ions sputters away the passivation layer. CF_x deposition and ion sputtering are surface processes whose rates do not depend on the passivation thickness for layers larger than 1 monolayer. Therefore, a steady-state passivation layer thickness is difficult to both computationally and experimentally obtain under anything other than coincidental conditions. A regulating process is required which depends on the thickness of the layer. In our mechanism, F atoms diffuse through the passivation to the underlying Si. The diffusing F atoms react with the polymer, etching it to form volatile CF_4. Since this is a bulk process and is dependent on the total thickness, a steady-state thickness of the passivation layer at each surface site can then be obtained.

The thickness of the passivation (in terms of number of layers L) is obtained from

$$\frac{dL}{dt}=\frac{1}{T}\left(\sum_i \Phi_i k_{ij}\theta_j-\sum_i \Phi_i^+ k_{ip}LT-[\text{F}]Lk_E\right)\quad (L<1), \tag{12a}$$

$$\frac{dL}{dt}=\frac{1}{T}\left(\sum_i \Phi_i k_{ip}-\sum_j \Phi_j^+ k_j T-[\text{F}]Lk_E\right)\quad (L>1), \tag{12b}$$

where T is the number of sites in a monolayer, [F] is the density of F atoms in the layer, Φ_i is the flux of passivating radicals, Φ_i^+ is the flux of incident ions, and σ_j is the density of surface sites not yet passivated. k_{is} is the sputtering probability, k_{ij} is the sticking coefficient for passivants on material j, k_{ip} is the sticking coefficient of passivants on the polymer, and k_E is the etching coefficient of the polymer for F atoms. We enforce that a surface site at a given spatial location cannot have more than a single layer of passivation until all sites have at least one layer. After a single layer of passivation is deposited, passivation grows on top of passivation.

In order for the incident F radicals to react with the Si surface covered by the passivation layer, five steps must take place: (1) F atoms adsorb on the top surface of the passivation layer. (2) The absorbed F atoms diffuse through the polymer layer to reach the polymer-Si interface. (3) The F atoms at the interface adsorb onto the Si surface. (4) The adsorbed F atoms passivate Si sites to form SiF_x. (5) SiF_x is desorbed (either spontaneously or by ion bombardment) and diffuses back through the polymer layer. The intermediate state in which F is at the interface and is then adsorbed onto Si appears somewhat artificial, though necessary to allow for a smooth transition between a clean Si surface and an Si surface fully covered by polymer. Assuming Fick's law for diffusion of F atoms through the passivation layer, the diffusion flux Γ_{F} reaching the Si surface is

$$\Gamma_{\text{F}}=D\frac{\text{F}_t-\text{F}_i}{L}, \tag{13}$$

where D is the diffusion coefficient, F_t is the F atom density on the top surface of the passivation layer, F_i is the F atom density at the interface between the polymer and Si, and L is the passivation layer thickness at that surface site.

At the polymer-Si interface, Si surface sites are sequentially passivated by F atoms to form either intermediate SiF_x sites, or a volatile SiF_4 product.

$$(Si)_s \xrightarrow{F_i} (SiF)_s \xrightarrow{F_i} (SiF_2)_s \xrightarrow{F_i} (SiF_3)_s \xrightarrow{F_i} (SiF_4)_g + (Si)_s . \quad (14)$$

Ion bombardment at any step during the sequential passivation process can release an etch product and free up a bare silicon site.

In writing these surface site balances, we have implicitly assumed that the number of sites, and hence area, of any given surface (e.g., silicon, top of polymer, interface) is constant. In reality, there is some amount of roughness and mixing at a surface due to ion bombardment, as illustrated by molecular dynamics simulations,[10] which increases the effective area of the surface. Although we have not addressed surface roughness in this model one could, in principle, account for its effects by including algorithms which track the surface roughness and adjust the number of surface sites accordingly. The issue is, in practice, somewhat more complicated. For example, based on geometrical arguments alone, not all sites in the roughened surface layer are equally accessible to species incident from the plasma. As a result, an accounting of microscopic transport through the roughened surface layer would also likely be required.

The coupled set of ordinary-differential equations for the time rate of change of surface coverages at each spatial location are integrated in time using a third-order Runge–Kutta technique. A summary of the surface reaction mechanism is in Table I. For the reasons discussed below, the variety of the species in the model has been constrained. For example, there is only a single polymerizing species, CF_2. This is a simplification. For example, experiments by Capps *et al.*[17] and Mackie *et al.*[18] have shown that, depending on reactor conditions and gas mixture, CF_2 can be either consumed or evolved at the surface of a growing polymer film. The latter result implies that the dominant polymer forming radical in their experiments is a species other than CF_2 and that CF_2 is chemically sputtered from the surface.

TABLE I. Surface reaction mechanism.

Species definitions:
- X_g: Gas phase species
- P_S: Surface site on top of polymer layer
- F_T: F adsorbed on top of polymer layer
- F_I: F adsorbed on Si or at the interface of Si and polymer
- F_A: Site on Si surface available for adsorption
- W_S: Reactor wall site
- R_S: Surface site available for polymer growth
- P: Polymer layer
- SiF_{XS}: Si site on surface passivated by x F atoms
- α: Fraction of Si sites overlayed by polymer
- T: Surface density of sites.

Reaction[a,b,c]	Probability	Note
$F_g + P_S \rightarrow F_T$	0.3α	
$F_g + P_S \rightarrow P_S + F_{2g}$	0.005α	
$F_g + P \rightarrow P + F_{2g}$	$0.005\,(1-P_S)$	
$CF_{2g} + R_S \rightarrow P + R_S$	0.3	
$CF_{3g} + P \rightarrow C_2F_{6g} + P$	$0.005\,\min(P,1)$	
$CF_{3g}^+ + P \rightarrow CF_{2g} + CF_3$	$p_0=0.1,\ E_T=150$ eV	d,e
$Ar_g^+ + P \rightarrow CF_{2g} + Ar$	$p_0=0.1,\ E_T=150$ eV	d,e
$F_T + P \rightarrow CF_{4g} + P_S$	$0.5T$	e
$F_T + F_A \rightarrow F_I + P_S$	$25T(F_T-F_A)F_A/\max(P,0.1)$	f
$F_g + F_A \rightarrow F_I$	$0.05(1-\alpha)$	
$F_g + F_A \rightarrow F_A + F_2$	$0.005(1-\alpha)$	
$F_I + SiF_{XS} \rightarrow SiF_{(X+1)S} + F_A$	$25T$	
$CF_3^+ + SiF_{XS} \rightarrow SiF_X + CF_{3g} + F_A$	1.0	f
$Ar^+ + SiF_{XS} \rightarrow SiF_X + Ar_g + F_A$	1.0	f
$F_g + SiF_{XS} \rightarrow F_{2g} + SiF_{XS}$	$0.005(1-\alpha)$	
$F_g + W_S \rightarrow F_{2g} + W_S$	0.005	
$CF_{2g} + W_S \rightarrow W_S$	0.8	f
$CF_{3g} + W_S \rightarrow C_2F_{6g} + W_S$	0.005	

[a]Unless otherwise specified, all ions neutralize on all surfaces, returning as their neutral counterparts.

[b]Processes not listed (e.g., $CF_{4g} + W_S \rightarrow$ Products) are nonreactive. Incident species reflect with unity probability.

[c]All gas phase species have units of flux ($cm^{-2}\,s^{-1}$). All surface species have units of fractional coverage. P has units of layers. Derivatives for surface species are divided by the surface site density, T. In this work, $T = 1\times10^{15}\,cm^{-2}$.

[d]See Eq. (8).

[e]Sum of probabilities of gas phase species with surface sites shown here may not sum to unity. The remaining probability is assigned to the incident species reflecting without reaction.

[f]Base case value. See text for sensitivity analysis.

III. C_2F_6 ETCHING OF Si

We applied the SKM model to the investigation of C_2F_6 etching of Si in the ICP reactor shown in Fig. 2. The reactor is cylindrical with a radius of 17 cm. The height of the plasma zone is 5.8 cm. Pure C_2F_6 or Ar/C_2F_6 is supplied from the shower head, ICP power at 13.56 MHz is applied using a four-turn coil and a 13.56 MHz bias is applied to the substrate. The gas pressure is 10 mTorr, the ICP power is 650 W and the total gas flow rate is 200 sccm. These parameters produce moderate, about 50%, dissociation on a reactor averaged basis using pure C_2F_6. No attempt was made to make the flux of reactants to the 20 cm diameter wafer uniform. The gas phase reaction chemistry is shown in Table II. Although the gas phase chemistry has, in reality, a larger variety of neutral and charged species (such as CF and CF^+) we have purposely chosen to use a more simplified gas phase mechanism. The intent is to minimize the variety species incident on the substrate in order to isolate specific processes to investigate their importance. A more complex gas phase reaction mechanism can be implemented as necessary. We will refer to polymer thickness in terms of number of layers, as opposed to actual thickness due to the uncertainty of the chemical structure of the film. For example, polytetrafluoroethylene, a $[C_2F_4]_n$ polymer, has mass density of 0.58 g/cm^3, which corresponds to approximately 6.6 A/layer, or 1.5 layers/nm.

Typical plasma properties are shown in Fig. 2 where the densities of CF_2 (deposition precursor), CF_3^+ (the major ion) and the etch product SIF_4 are plotted for the base case. The rf bias is 100 V and the time-averaged sheath potential is 95 V. The peak CF_2 density of $\approx 8\times10^{12}\,cm^{-3}$ occurs at the center of the reactor. Due to the power deposition peaking under the center of the coils, the CF_3^+ density has an off-axis peak of $\approx 3\times10^{11}\,cm^{-3}$. The density of the etch product is $\approx 3\times10^{12}\,cm^{-3}$ above the wafer and decreases as it diffuses into the plasma and is pumped away. The density of F atoms has

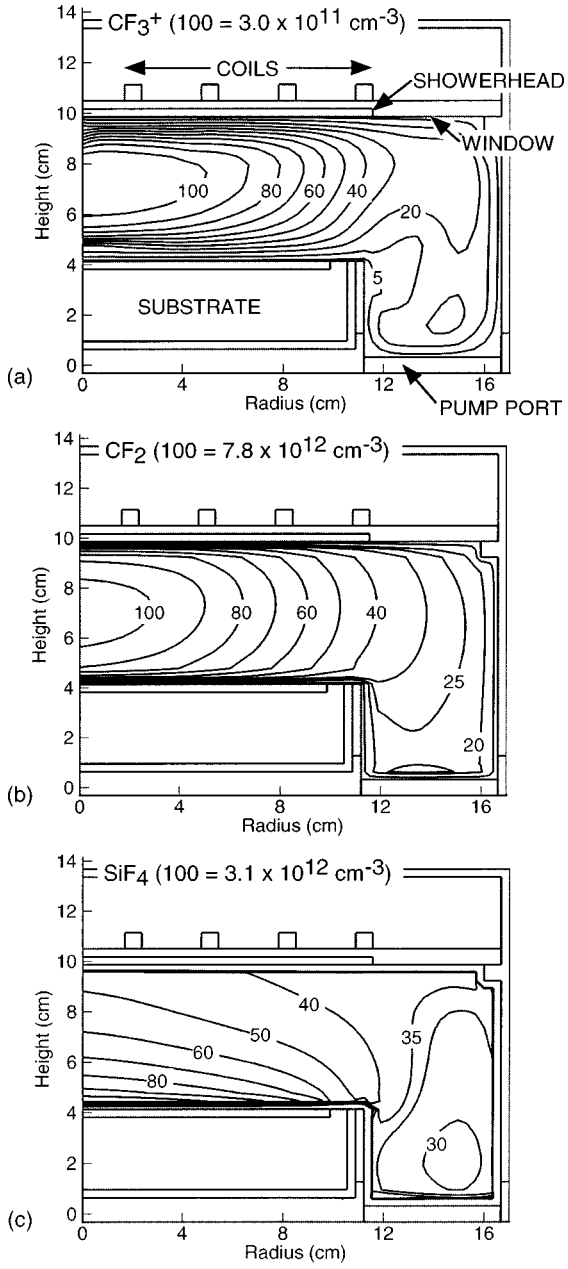

FIG. 2. Densities of (a) CF_3^+, (b) CF_2, and (c) SiF_4 in the ICP reactor for the base case conditions (10 mTorr, 650 W, 200 sccm, 100 V bias). The contours are labeled with the percentage of the maximum value shown at the top of each figure.

only a $\pm 10\%$ variation over the wafer with a peak value of $1.7\times 10^{13}\,\mathrm{cm}^{-3}$.

The fluxes of CF_2, CF_3^+, and F to the substrate are shown in Fig. 3(a). The reactive sticking coefficients of CF_2 and CF_3^+ on the walls of the reactor are, for this case, 0.8 and 1.0, respectively. The CF_3^+ flux has a small off-axis peak due to its off-axis source. With an ion flux of $\approx 1.2\times 10^{16}\,\mathrm{cm}^{-2}\,\mathrm{s}^{-1}$, the power onto the wafer is about $180\,\mathrm{mW\,cm}^{-2}$. Since F atoms have a smaller reactive sticking coefficient (0.005) on the walls, their density is more uniform, and produces a more uniform flux to the substrate. The predicted polymer thickness and etch rate for this case are shown in Fig. 3(b). As a consequence of the polymer forming CF_2 peaking on the axis, the polymer thickness on the wafer also peaks on axis. For these conditions, F atom etching of the polymer dominates and, since the F atom flux is uniform, the radial dependence of the polymer thickness is dominantly determined by the CF_2 flux. As the etch rate is flux limited by the diffusion of F atoms through the polymer layer, the etch rate is lowest on the axis where the polymer thickness is largest.

The total rate of deposition of CF_2 radicals on the reactor walls can be higher than that on the wafer since the area of the walls is typically larger. Therefore, as reactor wall conditions change, the CF_2 loss to the walls may have a larger influence on the plasma properties than the disposition of CF_2 on the wafer. For example, Schaepkens *et al.*[4] investigated the consequences of reactor wall temperature on the thickness of passivation layers, etch properties, and plasma properties in an ICP reactor operating in CHF_3 and C_3F_6. When the reactor wall temperature was changed from room temperature to $\approx 240\,^{\circ}\mathrm{C}$, they found a 40% increase in density for the CF_2 radical and a 10% decrease in density for the F atom radical based on plasma emission. The subsequent variation of the plasma properties modified the passivation thickness and ultimately the etch rate. Higher wall temperature produced more CF_2 in the plasma, thicker passivation and lower etch rates.

We simulated the change of reactor wall temperature by varying the CF_2 sticking probability (S_{CF_2}) on the chamber walls with the hypothesis that high wall temperature corresponds to low S_{CF_2}. The chord averaged densities of CF_2 radicals at midreactor (as would be observed by optical emission) are shown in Fig. 4 for $0.1 \leqslant S_{CF_2} \leqslant 0.8$. As S_{CF_2} increases, the CF_2 plasma density decreases which is a direct consequence of the higher CF_2 loss on the wall. The experimental results of Schaepkens *et al.* are also shown where we have assumed that $(1\text{-}S_{CF_2})$ scales as $T_w^{1/2}$. The steady-state passivation layer thickness and the etch rate as a function of radius on the wafer are shown in Figs. 5(a) and 5(b) for $S_{CF_2}=0.1-0.8$. The corresponding CF_2 fluxes, polymer thickness and etch rate at the center of the wafer are shown in Fig. 5(c). As the CF_2 sticking coefficient on the walls decreases, there is a corresponding increase in density of CF_2 and of its flux to the substrate. Lower sticking coefficients offer slightly more uniform fluxes. The polymer thickness also increases with decreasing S_{CF_2} in proportion to the increase in CF_2 flux, becoming somewhat more uniform at low sticking coefficient, in agreement with Schaepkens *et al.*[4] The rate of arrival of F atoms at the polymer-Si interface is inversely proportional to the passivation layer thickness. An increase of passivation layer thickness thus leads to a lower interface F atom density, and a decrease of the Si etch rate. The resulting etch rates vary inversely with the wall sticking coefficient and polymer thickness, becoming more uniform at lower wall sticking coefficients, in agreement with Schaepkens *et al.*

In high plasma density reactors, such as ICPs, rf substrate biases of $<$100s V typically do not contribute significantly to plasma generation. The bias does, however, determine the sheath potential, and so influences the etch process through the incident ion energy. To first order, the magni-

TABLE II. Ar/C_2F_6 reaction mechanism.[a] Species: $Ar, Ar^*, Ar^+, CF_4, CF_3^+, CF_3^-, CF_2, F, F^-, F_2, C_2F_6, C_2F_5, C_2F_4, C_2F_3, SiF_4, e$.

Reaction	Rate coefficient[b]	Reference
$e+Ar \rightarrow Ar^*+e$	c	19
$e+Ar \rightarrow Ar^+ + e + e$	c	20
$e+Ar^* \rightarrow Ar^+ + e + e$	c	21
$e+Ar^* \rightarrow Ar + e$	c	21
$e+CF_4 \rightarrow CF_3 + F^-$	c	22
$e+CF_4 \rightarrow CF_3^- + F$	c	22
$e+CF_4 \rightarrow CF_3 + F + e$	c	22
$e+CF_4 \rightarrow CF_3^+ + F + e + e$	c	22
$e+CF_4 \rightarrow CF_2 + F + F + e$	c	22
$e+CF_3 \rightarrow CF_2 + F + e$	c	22[d]
$e+CF_3 \rightarrow CF_2 + F^-$	c	22[d]
$e+C_2F_6 \rightarrow CF_2^+ + CF_3 + e + e$	c	23
$e+C_2F_6 \rightarrow CF_3 + CF_3^-$	c	23
$e+C_2F_6 \rightarrow C_2F_5 + F^-$	c	23
$e+C_2F_6 \rightarrow CF_3 + CF_3 + e$	c	23
$e+C_2F_6 \rightarrow CF_2 + CF_3 + e$	c	23
$e+C_2F_4 \rightarrow CF_2 + CF_2 + e$	c	23[e]
$e+C_2F_4 \rightarrow C_2F_4^+ + e + e$	c	23[e]
$e+C_2F_4 \rightarrow F^- + C_2F_3$	c	23
$e+CF_3^+ \rightarrow CF_2 + F$	2.0×10^{-8}	24[f]
$e+C_2F_5^+ \rightarrow CF_3 + CF_2$	2.0×10^{-8}	24[f]
$e+C_2F_4^+ \rightarrow CF_2 + CF_2$	2.0×10^{-8}	24[f]
$Ar^+ + Ar \rightarrow Ar + Ar^+$	1.0×10^{-9}	25
$Ar^+ + CF_4 \rightarrow CF_3^+ + F + Ar$	7.0×10^{-10}	25
$Ar^+ + CF_3 \rightarrow CF_3^+ + Ar$	7.0×10^{-10}	25
$Ar^+ + C_2F_6 \rightarrow CF_3^+ + CF_3 + Ar$	9.58×10^{-10}	25
$Ar^+ + C_2F_5 \rightarrow C_2F_5^+ + Ar$	1.0×10^{-10}	26[f]
$Ar^+ + C_2F_4 \rightarrow C_2F_4^+ + Ar$	1.0×10^{-10}	26[f]
$Ar^* + Ar^* \rightarrow Ar^+ + Ar + e$	5.0×10^{-10}	27
$Ar^* + CF_4 \rightarrow CF_2 + F_2 + Ar$	4.0×10^{-11}	28
$Ar^* + CF_3 \rightarrow CF_2 + F + Ar$	4.0×10^{-11}	28
$Ar^* + CF_2 \rightarrow CF + F + Ar$	4.0×10^{-11}	28
$Ar^* + C_2F_5 \rightarrow CF_2 + CF_3 + Ar$	4.0×10^{-11}	28
$Ar^* + C_2F_3 \rightarrow CF_2 + CF + Ar$	4.0×10^{-11}	28
$Ar^* + C_2F_6 \rightarrow CF_3 + CF_3 + Ar$	4.0×10^{-11}	28
$Ar^* + C_2F_4 \rightarrow CF_2 + CF_2 + Ar$	4.0×10^{-11}	28
$CF_3^+ + CF_3 \rightarrow CF_3^+ + CF_3$	1.0×10^{-9}	25
$CF_3^+ + C_2F_6 \rightarrow C_2F_5^+ + CF_4$	3.50×10^{-11}	25
$C_2F_5^+ + C_2F_5 \rightarrow C_2F_5^+ + C_2F_5$	1.0×10^{-9}	25
$C_2F_4^+ + C_2F_4 \rightarrow C_2F_4^+ + C_2F_4$	1.0×10^{-9}	25
$F^- + Ar^+ \rightarrow F + Ar$	1.0×10^{-7}	29
$F^- + CF_3^+ \rightarrow F + CF_3$	1.0×10^{-7}	29
$F^- + C_2F_4^+ \rightarrow F + C_2F_4$	1.0×10^{-7}	29
$F^- + C_2F_5^+ \rightarrow F + C_2F_5$	1.0×10^{-7}	29
$CF_3^- + Ar^+ \rightarrow CF_3 + Ar$	1.0×10^{-7}	29
$CF_3^- + CF_3^+ \rightarrow CF_3 + CF_3$	1.0×10^{-7}	29
$CF_3^- + C_2F_4^+ \rightarrow CF_3 + C_2F_4$	1.0×10^{-7}	29
$CF_3^- + C_2F_5^+ \rightarrow CF_3 + C_2F_5$	1.0×10^{-7}	29
$CF_3^- + F \rightarrow CF_3 + F^-$	5.0×10^{-8}	29
$F + F + M \rightarrow F_2 + M$	$2.4\times10^{-33}(T/298)^{0.033}\ cm^6\ s^{-1}$	30
$F + C_2F_4 \rightarrow CF_3 + CF_2$	4.0×10^{-11}	31
$F + C_2F_5 \rightarrow CF_3 + CF_3$	1.0×10^{-11}	31
$F + C_2F_3 \rightarrow C_2F_4$	1.0×10^{-12}	32
$F + CF_3 \rightarrow CF_4$	$1.99\times10^{-10}(T/300)^{-7.71}\exp(-1183.4/T)$	33
$F + CF_2 \rightarrow CF_3$	8.40×10^{-15}	31
$F_2 + CF_2 \rightarrow CF_3 + F$	4.56×10^{-13}	32
$F_2 + CF_3 \rightarrow CF_4 + F$	1.88×10^{-14}	32
$CF_3 + CF_3 \rightarrow C_2F_6$	7.67×10^{-12}	32
$CF_2 + CF_2 \rightarrow C_2F_4$	5.0×10^{-14}	32
$CF_2 + CF_3 \rightarrow C_2F_5$	8.26×10^{-13}	32

[a]Only reactions directly affecting species densities are shown here. Additional electron impact collisions (e.g., momentum transfer, vibrational excitation) are included in the EETM.
[b]Rate coefficients have units $cm^3\ s^{-1}$ unless noted otherwise.
[c]Computed using the electron energy distribution and electron impact cross section from cited reference.
[d]Estimated by analogy to CF_4.
[e]Estimated by analogy to C_2F_6.
[f]Estimated. See cited reference for similar reaction.

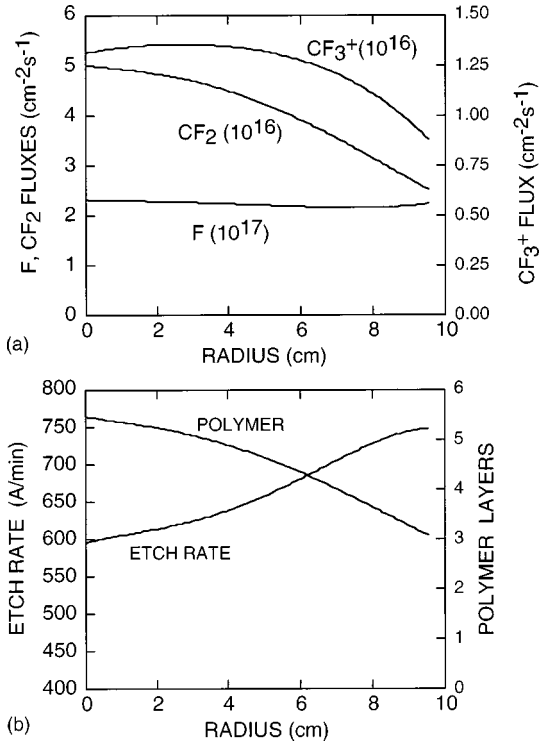

FIG. 3. Plasma and surface properties for the base case as a function of radius: (a) Fluxes of CF_3^+, CF_2, and F to the wafer. (b) Polymer layers and etch rates. The etch rate is constrained by the diffusion of F atoms through the polymer layer, giving rise to a minimum at the center of the wafer where the polymer layer is thickest.

tudes of all reactive fluxes are insensitive to the magnitude of the bias. Changing the bias only changes the energy of the ions striking the substrate, which, for this reaction mechanism, only affects the sputtering rate of the polymer and the rate of ion activated desorption of etch products. We varied the rf substrate bias from 50 to 150 V to vary the time-averaged sheath potential and show the resulting polymer thickness and etch rate as a function of time-averaged sheath potential in Fig. 6. Only the rate of polymer sputtering was allowed to change. As the bias and sheath potential increase,

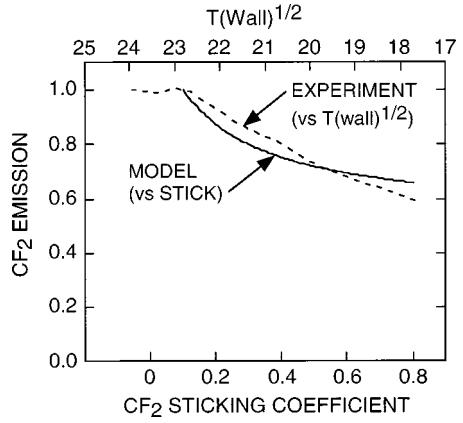

FIG. 4. Simulated CF_2 emission as a function of the sticking coefficient of CF_2 radicals on the reactor walls. Experimental results of Schaepkens *et al.* (see Ref. 4) are shown plotted as a function of $T(\text{wall})^{1/2}$. A decreasing sticking coefficient for CF_2 increases its gas phase density.

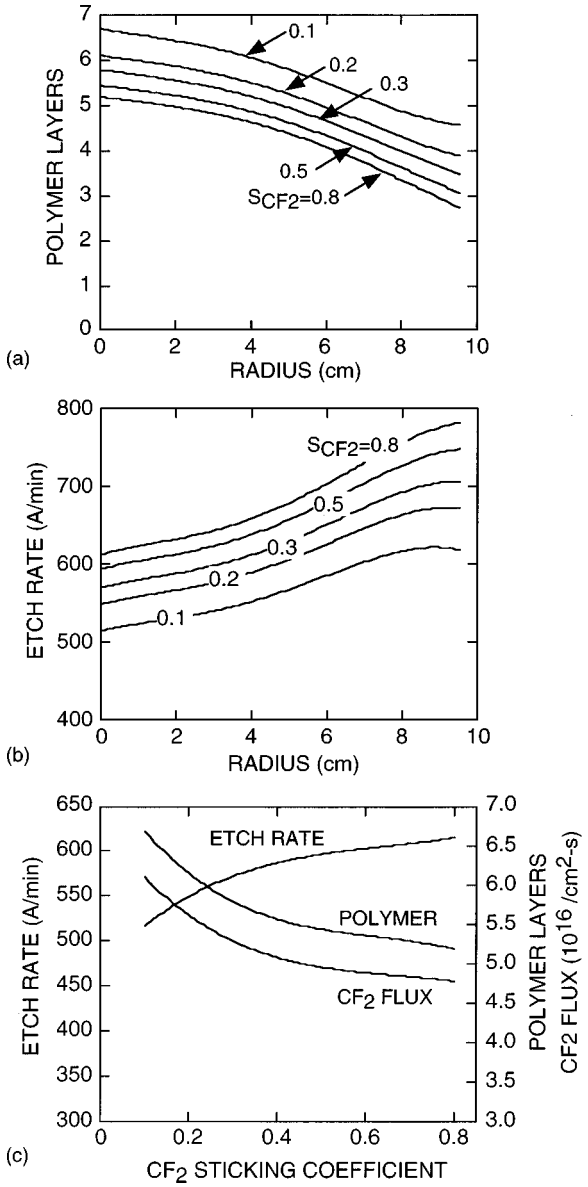

FIG. 5. Surface properties as a function of CF_2 sticking coefficient (S_{CF_2}) on the walls of the reactor. (a) Polymer layers as a function of radius for different sticking coefficients. (b) Etch rates for different sticking coefficients. (c) Polymer layers, CF_2 flux and etch rate at the center of the wafer as a function of S_{CF_2}. Decreasing S_{CF_2} produces thicker polymer layers, lower etch rates and a somewhat more uniform etch rate profiles.

the ion energy incident on the passivation layer increases thereby increasing the polymer erosion rate. The end result is a thinner polymer thickness and a higher etch rate.

Many of the transport coefficients and reaction rate coefficients used in our surface reaction mechanism are estimated or derived from parametric studies. Typically, in the absence of comprehensive fundamental measurements of these coefficients or coefficients derived from molecular dynamics simulations, the coefficients are derived by parameterizing the model and comparing predicted etch rates and polymer thicknesses to well characterized experiments. This methodology has been successfully used in deriving surface reaction rate coefficients for surface profile models by Vahedi *et al.*[33]

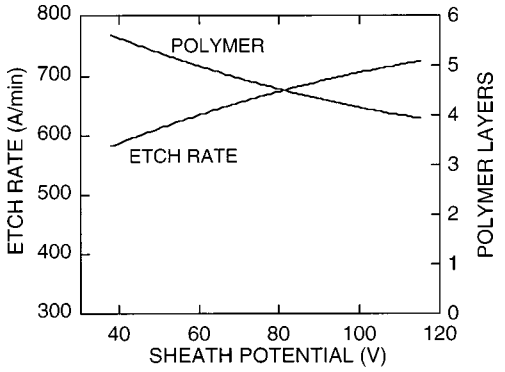

FIG. 6. Polymer thickness and etch rate at the center of the wafer as a function of sheath potential. Increased sputtering of the polymer layer with increasing bias decreases its thickness and increases the etch rate.

Given the method of selecting coefficients for the model, it is valuable to investigate the sensitivity of the model to variations in those coefficients. For example, the probability of polymer sputtering by ions is given by Eq. (8). In the results thus far, we chose $p_0=0.1$ and $E_r=150$ eV. The etch rate and polymer thickness as a function of p_0 are shown in Fig. 7(a). As p_0 decreases the polymer thickness increases and the etch rate decreases. At $p_0=0$, the polymer thickness is 8.2 layers. There is not unlimited polymer growth, and there is still a net etch rate, since the polymer continues to be etched by F atoms. The sensitivity of the silicon etch rate and polymer thickness to the rate of polymer etching by F atoms is shown in Fig. 7(b). The base case value is 0.5 s^{-1}. Without polymer etching by F atoms, the polymer is 16.6 layers thick. As the polymer etch rate increases, the polymer thickness decreases and the etch rate increases, though not at the rate one might expect based solely on the decrease in polymer thickness. This trend results from the fact that F atoms which would otherwise be available to diffuse through the polymer layer are being depleted by their etching of the polymer. The sensitivity of silicon etch rate and polymer thickness on the rate of diffusion of F atoms through the polymer is shown in Fig. 7(c). (The base case has speed 25 layers/s.) Increasing rates of diffusion result in higher etch rates. There is an initial linear rate of increase in the etch rate with diffusion speed until all of the silicon surface sites are saturated. At that time the etch rate is limited by desorption of etch product. The polymer thickness experiences a small increase as the F atom diffusion speed increases. This results from there being a shorter residence time for F atoms in the polymer, and so there being less likelihood to etch the polymer.

The predicted etch rate is also sensitive to the details of the etch model embodied, in part, in the identity of the etch products. In the absence of physical sputtering, Si sites are passivated by F atoms, forming chemisorbed $\equiv SiF_n$. For $n\leqslant 3$, some amount of ion activation is likely required to remove the SiF_n etch product from the surface. If we assign a sufficiently high probability for ion desorption so that etching is not severely constrained by the desorption step, there is not an acute sensitivity of etch rate on the etch product. For example, assigning a unity ion activated desorption probability for the $-SiF_3 \rightarrow SiF_4$ passivation step, as in the base case, the etch rate is 596 A/min. Adding a 0.5 ion activated

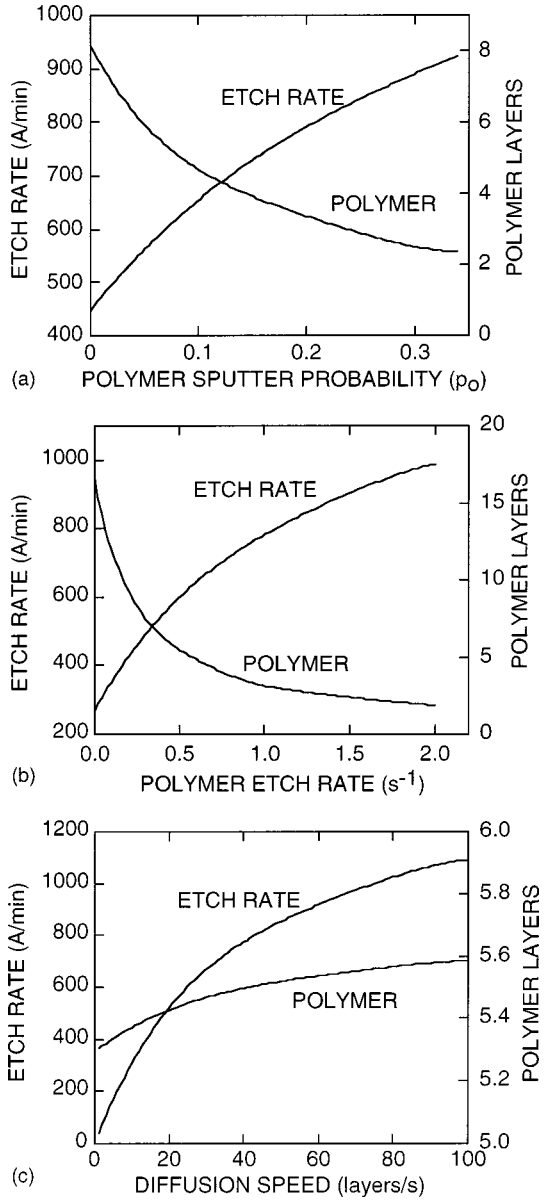

FIG. 7. Results from a sensitivity study of etch rates and polymer thickness while varying rate coefficients in the surface reaction mechanism. (a) Polymer sputter probability (base case has $p_0=0.1$), (b) Polymer etch rate by F atoms (base case has $k=0.5\,s^{-1}$), (c) F atom diffusion rate (base case=25 layers/s).

desorption probability for $\equiv SiF_3$ raises the etch rate to 667 A/min. Adding an additional 0.25 ion activated desorption probability for $\equiv SiF_2$ increases the etch rate to 739 A/min. The weak dependence of etch rate on the details of the etch product is, for these conditions, a consequence of the fact that the F atom flux and F atom diffusion rates through the polymer are sufficiently high that passivation of the surface is not rate limited by the availability of fluorine.

Where the etch rate may, in fact, be sensitive to the identity of the etch product is in the ion activated desorption step. There is a complex, and not well understood, mechanism for transfer of ion energy through the polymer to activate the desorption. The mechanism could be either kinematic, thermal or a combination of the two. To investigate the sensitivity of etch rate on ion activated desorption, the

probability for ion desorption was varied between 0.05 and 1.0. The resulting etch rates as a function of position are shown in Fig. 8(a) for the base case. The etch rate at $r=0$ and the Si_s surface coverage (Si sites which are not passivated) are shown in Fig. 8(b). Recall that the polymer thickness is largest at $r=0$ and decreases to larger radii as shown in Fig. 3. For high probabilities of ion activated desorption, the etch rate is not limited by the desorption step but rather by the rate of diffusion of F atoms through the polymer. The etch rate is therefore smallest on axis. The Si_s surface coverage is large, 0.2 for unity ion activation, indicating that as Si sites are passivated by F atoms, they are rapidly etched, leaving a reasonably large fraction of sites available for repassivation. As the ion activated desorption probability decreases, the etch rate becomes progressively more limited by the rate of desorption, as opposed to the rate of passivation. The etch rate transitions from being largest at large radii, where the polymer is thinnest, to being largest at small radii, where the ion flux is largest. There is a commensurate decrease in the etch rate. The degree to which the etch rate is limited by ion activated desorption is indicated by the Si_s surface coverage. At low values of the ion activated desorption, for example 0.1, the Si_s surface coverage is less than 0.03, indicating that nearly all sites are passivated and ''waiting'' for ion activated desorption.

The Si etch rate is ultimately a first order function of three fluxes: the ion flux, the polymerizing precursor (in this case, CF_2) and the F atom flux. For otherwise constant conditions, the etch rate varies inversely with the thickness of the polymer layer, and all three fluxes contribute to determining the thickness of the polymer layer. The F atom and ion flux decrease its thickness through etching and sputtering, while the CF_2 flux adds to its thickness. The ion flux also desorbs the etch product. Unless there is severe depletion of the feedstock C_2F_6, it is difficult to significantly change the ratios of these fluxes since varying power or pressure changes all fluxes in approximately the same proportion.

One can, however, change the relative proportions of these fluxes by varying the gas mixture. For example, while keeping pressure, power deposition, and total flow rate constant (10 mTorr, 650 W, 200 sccm), the gas mixture was varied from $Ar/C_2F_6=0/100$ to 95/5. The resulting fluxes, etch rates and polymer thickness are shown in Fig. 9. By diluting the C_2F_6 with argon, the fluxes of F and CF_2 to the substrate generally decrease, though at a slower rate than the decrease in C_2F_6 mole fraction. This results from the plasma density and electron temperature increasing with decreasing C_2F_6 mole fraction. The lower flow rate of C_2F_6 is compensated by the higher electron density, thereby producing commensurate dissociation rates of C_2F_6. In fact, the CF_2 flux actually peaks at an intermediate mole fraction of C_2F_6 for this reason.

Due to the increase in the ion flux (which erodes the polymer layer) and overall decrease in the CF_2 flux (which builds the polymer layer), the ratio of the (ion flux)/(CF_2 flux) increases with increasing Ar dilution. The polymer thickness therefore decreases with increasing Ar dilution. When the etch rate is constrained by diffusion of F atoms through the polymer, the etch rate increases with decreasing

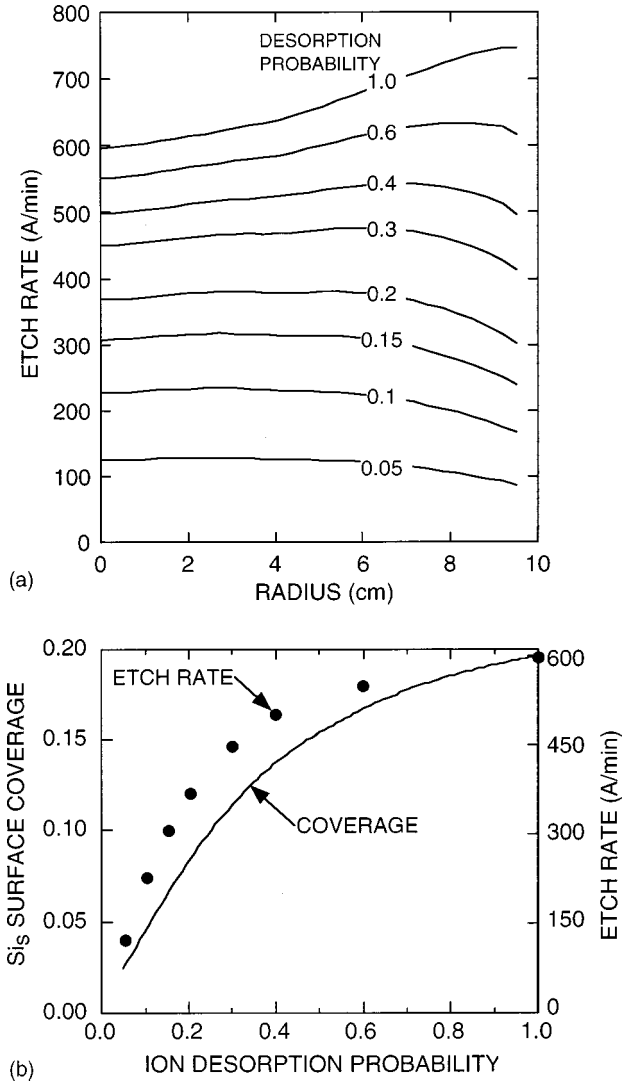

FIG. 8. Surface properties as a function of the ion desorption probability of the etch products. (a) Etch rate as a function of radius for different desorption probabilities. (b) Etch rate and coverage of Si_s at the center of the wafer as a function of ion desorption probability. At high desorption probability, the etch rate is limited by the diffusion of F atoms through the polymer. At low ion desorption probabilities, the etch rate is limited by the ion flux.

polymer thickness provided that the F atom flux is above a critically high value which saturates the Si surface sites. As the F atom flux decreases below this value, the etch rate decreases in spite of a decrease in the polymer thickness. For these conditions, the maximum in etch rate occurs at $Ar/C_2F_6=0.8/0.2$ where the polymer layer is thin but the F atom flux has not decreased below its critical value. Although the etch rate maximizes at this low C_2F_6 mole fraction, desirable etch characteristics such as selectivity and low lateral etch rates, which largely depend on polymer layers, will degrade with increasing Ar dilution.

IV. CONCLUDING REMARKS

SKM was developed in the framework of the HPEM to investigate plasma-surface interactions. The SKM employs a time-dependent surface-site-balance model, modified to allow for overlying polymer layers. The SKM obtains fluxes of

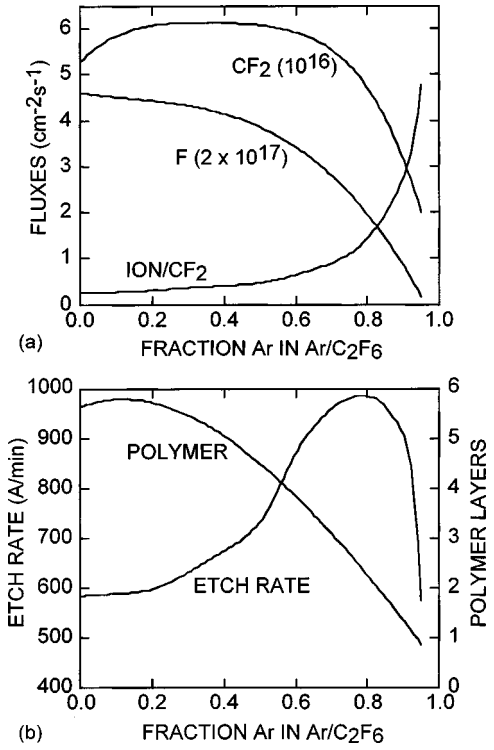

FIG. 9. Plasma and surface properties as a function of dilution with argon in an Ar/C_2F_6 gas mixture. (a) Fluxes of CF_2, F atoms and the ratio of the ion flux to the CF_2 flux. (b) Etch rate and polymer thickness. The etch rate increases with decreasing polymer thickness until the F atom flux is insufficient to fully passivate silicon sites.

reactants from the HPEM, implements a specified surface reaction mechanism and produces surfaces coverages as function of position at the plasma-surface interface. Results from the SKM are used to update reactive sticking coefficients and the species returning to the plasma for use in the remainder of the HPEM. The model was used to investigate Ar/C_2F_6 etching of Si in a high plasma density ICP reactor. Results demonstrated that with a decreasing CF_2 sticking coefficient on the reactor wall, the bulk CF_2 density increases, which leads to a thicker polymer layer on the wafer and a lower Si etch rate. Higher biases produce larger sputtering rates and thinner passivation. A sensitivity analysis was performed on rate coefficients employed in the model. Both the magnitude and radial dependence of the etch rate depend on the rate of ion activated desorption of etch products. For conditions where ion desorption is not rate limiting, etch rates generally vary inversely with polymer thickness. For conditions where ion desorption is rate limiting, the etch rate and its spatial dependence varies with ion flux. A topic for further study is the mechanism whereby ions deliver activation energy through polymer layers to the underlying silicon.

ACKNOWLEDGMENTS

This work was supported by the Semiconductor Research Corporation, Applied Materials, and LAM Research Corporation.

[1] J. T. C. Lee, N. Layadi, K. V. Guinn, H. L. Maynard, F. P. Klemens, D. E. Ibbotson, I. Tepermeister, P. O. Egan, and R. A. Richardson, J. Vac. Sci. Technol. B **14**, 2510 (1996).
[2] B. E. E. Kastenmeier, P. J. Matsuo, G. S. Oehrlein, and J. G. Langan, J. Vac. Sci. Technol. A **16**, 2047 (1998).
[3] K. Nishikawa, T. Oomori, and K. Ono, J. Vac. Sci. Technol. B **17**, 127 (1999).
[4] M. Schaepkens, R. C. M. Bosch, T. E. F. M. Standaert, and G. S. Oehrlein, J. Vac. Sci. Technol. A **16**, 2099 (1998).
[5] T. E. F. M. Standaert, M. Schaepkens, N. R. Rueger, P. G. M. Sebel, G. S. Oehrlein, and J. M. Cook, J. Vac. Sci. Technol. A **16**, 239 (1998).
[6] N. R. Rueger, J. J. Beulens, M. Schaepkens, M. F. Doemling, J. M. Mirza, T. E. F. M. Standaert, and G. S. Oehlein, J. Vac. Sci. Technol. A **15**, 1881 (1997).
[7] W. Z. Collison, T. Q. Ni, and M. S. Barnes, J. Vac. Sci. Technol. A **16**, 100 (1998).
[8] N. Mantzaris, A. Boudouvis, and E. Gogolides, J. Appl. Phys. **77**, 6169 (1995).
[9] E. Meeks, R. S. Larson, S. R. Vosen, and J. W. Shon, J. Electrochem. Soc. **144**, 357 (1997).
[10] B. A. Helmer and D. B. Graves, J. Vac. Sci. Technol. A **16**, 3502 (1998).
[11] D. E. Hanson, A. F. Voter, and J. D. Kress, J. Appl. Phys. **82**, 3552 (1997).
[12] M. J. Grapperhaus and M. J. Kushner, J. Appl. Phys. **81**, 569 (1997).
[13] S. Rauf and M. J. Kushner, J. Appl. Phys. **83**, 5087 (1998).
[14] A. J. Bariya, C. W. Frank, and J. P. McVittie, J. Electrochem. Soc. **137**, 2575 (1990).
[15] S. Samukawa and S. Furuoya, Jpn. J. Appl. Phys., Part 2 **32**, L1289 (1993).
[16] C. F. Abrams and D. B. Graves, J. Appl. Phys. **86**, 2263 (1999).
[17] N. E. Capps, N. M. Mackie, and E. R. Fisher, J. Appl. Phys. **84**, 4736 (1998).
[18] N. M. Mackie, V. A. Venturo, and E. R. Fisher, J. Phys. Chem. B **101**, 9425 (1997).
[19] K. Tachibana, Phys. Rev. A **34**, 1007 (1986).
[20] D. Rapp and P. Englander-Golden, J. Chem. Phys. **43**, 1464 (1965).
[21] R. H. McFarland and J. D. Kinney, Phys. Rev. **137**, A1058 (1965).
[22] R. A. Bonham, Jpn. J. Appl. Phys., Part 1 **33**, 4157 (1994).
[23] M. Hayashi, in *Gaseous Dielectrics V*, edited by L. G. Christophorou and D. W. Bouldin (Pergamon, New York, 1987).
[24] M. Hayashi and T. Nimura, J. Appl. Phys. **54**, 4879 (1983).
[25] E. Fisher, M. E. Weber, and P. B. Armentrout, J. Chem. Phys. **76**, 4932 (1982).
[26] G. K. Jarvis, C. A. Mayhew, and R. P. Tuckett, J. Phys. Chem. **100**, 17166 (1996).
[27] P. K. Leichner and R. J. Ericson, Phys. Rev. A **9**, 251 (1974).
[28] J. E. Velazco, J. H. Koltz, and D. W. Sester, J. Chem. Phys. **65**, 3468 (1976).
[29] R. E. Olson, J. R. Peterson, and J. Moseley, J. Chem. Phys. **53**, 3391 (1971).
[30] E. L. Duman, N. P. Tishchenko, and I. P. Shmatov, Dokl. Phys. Chem. **295**, 5 (1987).
[31] I. C. Plumb, K. R. Ryan, Plasma Chem. Plasma Process. **6**, 205 (1986).
[32] D. R. F. Burgess, Jr., M. R. Zachariah, W. Tsang, and P. R. Westmoreland, Prog. Energy Combust. Sci. **21**, 453 (1996).
[33] V. Vahedi, D. J. Cooperberg, J. M. Cook, L. Marquez, E. Hudson, and J. Winniczek, 45th International Symposium of the American Vacuum Society, Baltimore, MD, November 1998, Paper PS2-TuM9.